Microstructure and texture evolution of the non-oriented silicon steel during punching

Xiang Fang, Wei Wang, François Brisset, Anne-Laure Helbert, Thierry Baudin

Microstructure and texture evolution of the non-oriented silicon steel during punching

Xiang Fang[a,b,c,d], Wei Wang[a,b,c,d,*], François Brisset[e], Anne-Laure Helbert[e], Thierry Baudin[e]

[a]School of Automotive Engineering, Wuhan University of Technology, Wuhan, 430070, China

[b]Hubei Key Laboratory of Advanced Technology for Automotive Components, Wuhan University of Technology, Wuhan 430070, China

[c]Hubei Collaborative Innovation Center for Automotive Components Technology, Wuhan University of Technology, Wuhan 430070, China

[d]Hubei Research Center for New Energy & Intelligent Connected Vehicle, Wuhan University of Technology, Wuhan 430070, China

[e]Université Paris-Saclay, CNRS, Institut de chimie moléculaire et des matériaux d'Orsay, Orsay, France.

Abstract: The iron core of motors is mainly manufactured using a punching process from rolled non-oriented silicon steel, and this leads to deformation and texture evolution at cutting edge. According to this, circular samples of a non-oriented silicon steel were prepared by punching with blunt punch tools. In this work, two positions along the RD and TD directions at the cutting edge were analyzed. The main mechanisms of deformation for both positions are dislocation slip and formation of shear bands. These two mechanisms lead to similar texture evolutions for both positions. The dislocation slip leads to the formation of the $\{221\}\langle uvw\rangle$ component in the unbending area (200 μm away from cutting edge) and in the intermediate continuum bent area. In addition, the evolution of the texture from the $\{111\}$ γ fiber to the $\{110\}$ fiber was observed at the extremity of the cutting edge with formation of shear bands.

Keywords: Microstructure, Texture, Non-oriented silicon steel, Punching

1. Introduction

Non-oriented silicon steels are still the main manufacturing materials of motor core. This type of materials has excellent properties as low iron loss and high magnetic permeability are required to ensure performance of motors. It is known that the crystal of silicon steel exhibits magnetic anisotropy. The <100> crystallographic directions are the most easily magnetized ones, the <110> directions being the seconds and the most difficult magnetized directions are the <111> [1]. Therefore, the {100}<uvw> fiber is the optimal grain orientation, in which the other two <100> directions could be uniformly distributed in the rolling plane of the material.

As mentioned above, the texture of silicon steels has an important influence on its magnetic properties. For this reason, there are many studies on texture evolution of silicon steel sheets. Some studies are focused on the initial texture, controlled during the casting process [2, 3]. Some other researches aims to at improve the texture with optimization of the process and related parameters after casting, as rolling direction of cold rolling [4-6], reduction rate of hot rolling [7], temperature of rolling process [8], annealing temperature after cold rolling [9, 10], two-stage cold rolling process and related parameters [11]. There are also studies dealing with the effects of material composition on texture control [12]. However, all these studies are mainly conducted to either enhance the texture components as {001}<uvw>, and especially {001}<100>, {001}<uv0> and {0kl}<100> orientations, or to reduce the {111}<uvw> components and thus improve the material magnetic properties.

At present, considering the efficiency factor, the factories mainly use the punching process to manufacture iron core. This process can lead to a strong plastic deformation zone of 0.3 to 0.5 mm width at the cutting edge [13, 14]. Meanwhile, Saleem et al. [15] research shows that the microstructure at cutting edge is heterogeneous with formation of ribbon grains and shear bands. All these studies reveal

that there should be a change of local texture at the cutting edge of material, thus affecting the performance of iron core. According to this assumption, the deformation mechanisms and related texture evolution of non-oriented silicon steels at the cutting edge after punching is studied in this paper.

2. Materials and Methods

The non-oriented silicon steel produced by China Baowu Steel Group Corporation Limited was used during this study. The main chemical composition of the material is shown in Table 1 and the thickness of the sheet is 0.5 mm. Circular samples of 30 mm in diameter are obtained from the material sheet using a punching process with 4% as the clearance. The punching experiments were performed by the help of a hydraulic press with 5 tons as the maximum force. During the punching, the displacement of the press head was of about 13 mm/s. Generally, the cutting surface after punching with sharp tools is almost plat with a small burr. The area near the cutting edge with strong deformation is very narrow. On the contrary, the punching with blunt tool introduces a wider deformation area and a larger burr at the cutting edge [14]. For a detailed study of the texture evolution from the cutting edge to the inner of the material, a worn punch tool was selected. The punching process geometry and the dimensions of mold are described in Fig. 1.

Table 1: Chemical composition of the material.

Elements	Si	Al	Fe
Fractions (wt%)	0.63	0.23	Bal.

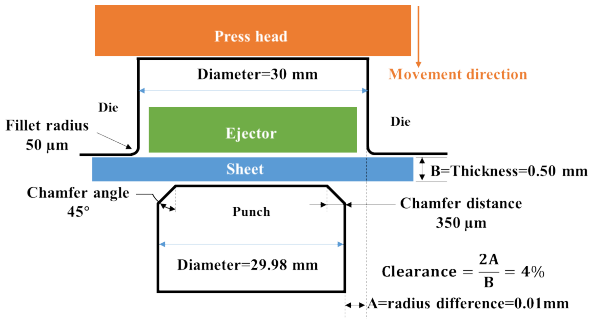

Fig. 1: Geometrical description of the punching process and dimensions of the mold.

Two positions of the circular samples at cutting edge were studied, as shown in Fig.2a. One position corresponds to the point indicated by the rolling direction (RD) and the other is that indicated by the transverse direction (TD). For each position, some specimens are cut from the circular samples, as shown in Fig.2b, and the related surface RD (or TD)-ND (normal direction) is studied. In the present paper, the studied positions will be named as specimen-RD or specimen-TD.

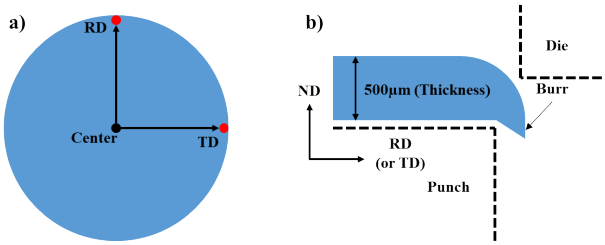

Fig. 2: a) Illustration of the positions analyzed (red points); b) surface studied for each position.

During this study, microstructure and texture of cutting edge are analyzed by electron backscatter diffraction (EBSD) using a field emission gun-scanning electron microscope (FEG-SEM, ZEISS Supra 55 VP) fitted with an EDAX Velocity EBSD system. Before the EBSD analysis, specimens with burrs were grounded with SiC paper. Then, they were polished gradually with diamond polishing fluids of 3 µm, 1 µm and 0.5 µm. Finally, they were polished and etched with an oxide polishing suspension (0.02 µm, OPU, Struers). The resolution of most EBSD analyses is of 1 µm as the step size. To obtain more detailed information on the substructure inside grains, some EBSD analyses were carried out with a 0.2 or 0.5 µm step size.

Microstructures and textures of samples were analyzed using TSL-EDAX OIM™ Analysis software. In order to prevent symmetry errors during the calculation of the orientation distribution function (ODF), the intervals of φ1, Φ and φ2 were chosen as 360°, 90° and 90°, respectively (triclinic symmetry). In addition, the harmonic method was used and the series rank of calculation was set as 34 [16].

3. Results and discussion

3.1 Microstructure evolution during punching

The initial microstructure of the material before punching is shown in Fig. 3. Grains of this material are equiaxed and the average grain size is 25.7 μm. There is no color gradient inside the grains (Fig. 3a). The average value of grain orientation spreads (GOS), which is a quantitative estimation of intragranular misorientation [17], is 0.45 for the initial material. All these reveal that this material is completely recrystallized before the punching process. Moreover, some grain boundaries with low misorientation angle could be observed in the grains (Fig. 3b). The fractions of low angle grain boundaries (LAGB) 2°-5°, 5°-15° and high angle grain boundaries (HAGB) are 4.6%, 11.5% and 83.9%, respectively. The Mackenzie random distribution describes the misorientation distribution of grain boundaries for a randomly oriented cubic material [18], and it is always applied as a reference. Compared to this random distribution, the smaller the average misorientation of grain boundaries is, the sharper the texture of material is [19]. Therefore, as shown in Fig. 3c, the initial material used in this study should have a certain texture and not be random.

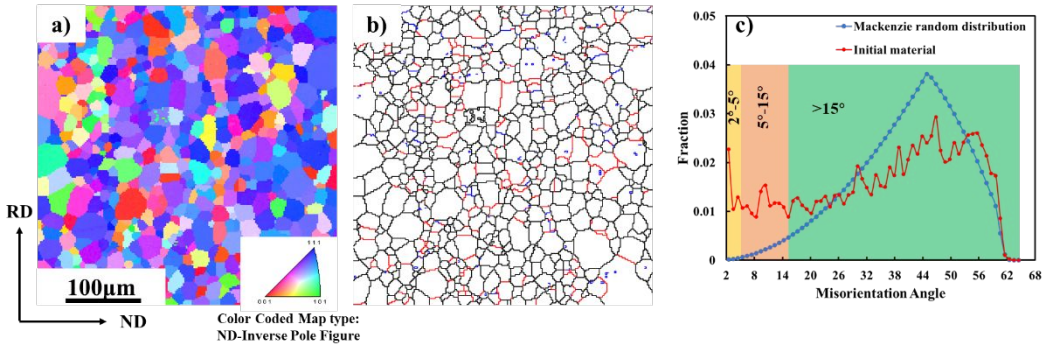

Fig. 3: a) Inverse Pole Figure (IPF) map of the initial non-oriented silicon steel before punching; b) Blank map of a) with grain boundaries (misorientation >15°); blue and red lines show the LAGBs (2°< misorientation <5°) and LAGBs (5°< misorientation <15°), respectively; c) Misorientation angle distribution of grain boundaries in the initial material, compared to the Mackenzie random distribution.

After punching, the deformed microstructure of the material was analyzed. Fig. 4 shows the microstructure of the cutting edges for the specimens-RD and TD. Macroscopically, the upper surface of both specimens shows an arc-shape as shown with yellow dotted lines shown in Fig. 4a and b. This indicates the existence of bending for both specimens during punching.

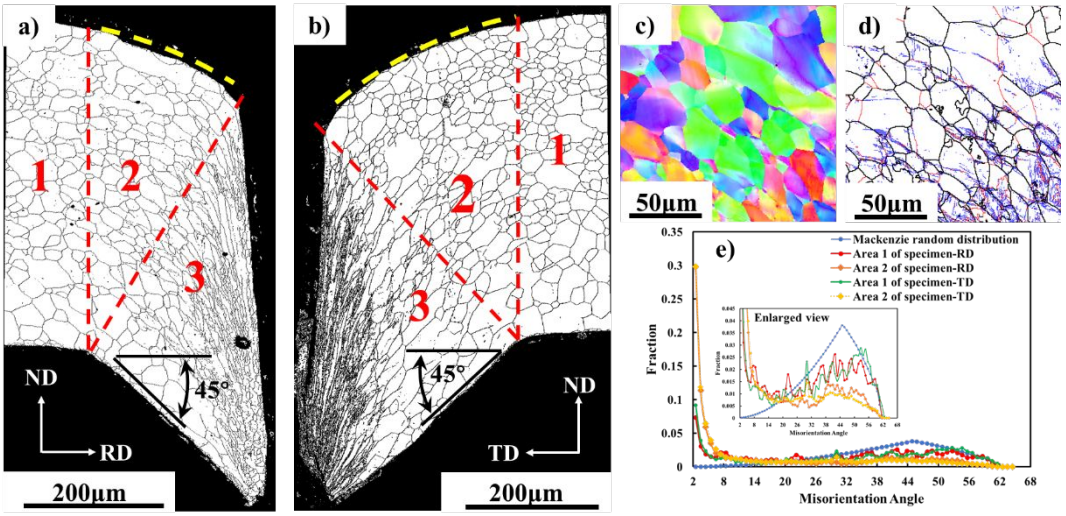

Fig. 4: Blank map with grain boundaries (misorientation >15°) of a) specimen-RD and b) specimen-TD, yellow dotted lines show the bending trend of upper surface; c) IPF+IQ map of a crop area from area 2 of one specimen-RD with a high resolution (step size: 0.5 µm); d) Blank map of c) with grain boundaries

(misorientation >15°), blue and red lines show respectively the LAGBs (2°< misorientation <5°) and LAGBs (5°< misorientation <15°); e) Misorientation angle distribution of grain boundaries in area 1 and area 2 of both specimens; RD, TD and ND in a) and d) represent the sample directions before punching.

According to the coordinate system of the initial sheet, three areas could be observed in both specimens. The area 1 is almost 200 µm away from cutting edge. The bottom surface of this area is horizontal and the bent angle of its upper surface is less than 5°. Therefore, it can be considered that the bending in this area is negligible. Microscopically, this area contains mainly equiaxed grains as shown in initial material. The area 2 corresponds to the bending zone with a rotation around the bend point. In this area, grains are slightly elongated and rotated. Using high resolution analysis (Fig. 4c), the presence of color gradient is observed in the grains of area 2. In addition, compared to the initial material, the fraction of LAGBs with 2-5° misorientation increases for the areas 1 and 2 (Fig. 4d and e).

The area 3 is close to the cutting edge with a straight bottom surface, whose tilt angle is about 45° relative to the horizontal direction. This angle corresponds to a cumulative bending angle of area 2 and equals to the chamfer angle of the punch. Moreover, the ribbon grains could be observed at the extremity of the cutting edge as in another study [15]. These grains were mainly deformed by shear effect at cutting edge during punching. Therefore, in this area, there are a non-negligible bending effect and a shearing effect.

3.2 Texture evolution during punching

As mentioned earlier, the bending of area 1 could be considered negligible. On the contrary, the areas 2 and 3 of both specimens are bent from initial sheet.

The bending has two effects on the grain orientation. Firstly, the bending can rotate the grain through deformation. Secondly, the bending effect rotates the specimen along the bending axis. This rotation changes the orientation of the initial sample system relative to the detector system, and has obviously an influence on the orientation analysis [20]. Therefore, the EBSD data of areas 2 and 3 need to be corrected before studying the texture evolution.

As the bending angle varies for all pixels in the area 2 (Fig. 5), the pixel rotation method (PRM) proposed in the literature [20] was applied for the EBSD data correction in this area. For every single pixel, the bending angle θ as shown in Fig. 5 is calculated. Subsequently, a reverse rotation of θ is applied to correct the orientation of the corresponding pixel.

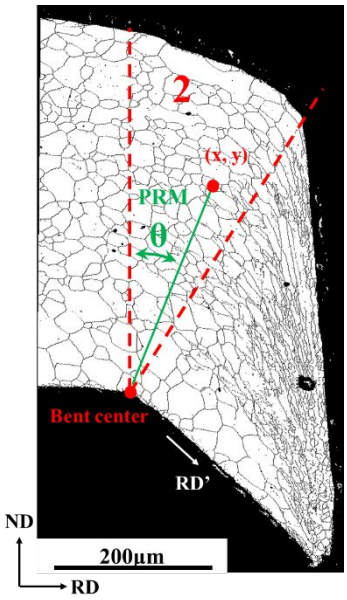

Fig. 5: Illustrations of the sample geometry, and of the correction of the sample system by the pixel rotation method (PRM).

The bottom surfaces of area 3 are straight for both specimens, and the bent angles are 45° relative to initial direction. This indicates the sample system of the whole area 3 rotated 45° without difference between pixels. Therefore, the EBSD data are corrected with a direct rotation of whole area for both specimens.

The analysis of GOS parameter demonstrates that the deformation of area 2 is higher than that of area 1, for both specimens. However, the difference of average values between the two areas is small (Fig. 6). Moreover, these values are less than 5° which is consistent with the results of Fig. 4c and indicates a weak deformation and so the main deformation mechanisms for both areas should be dislocation slip.

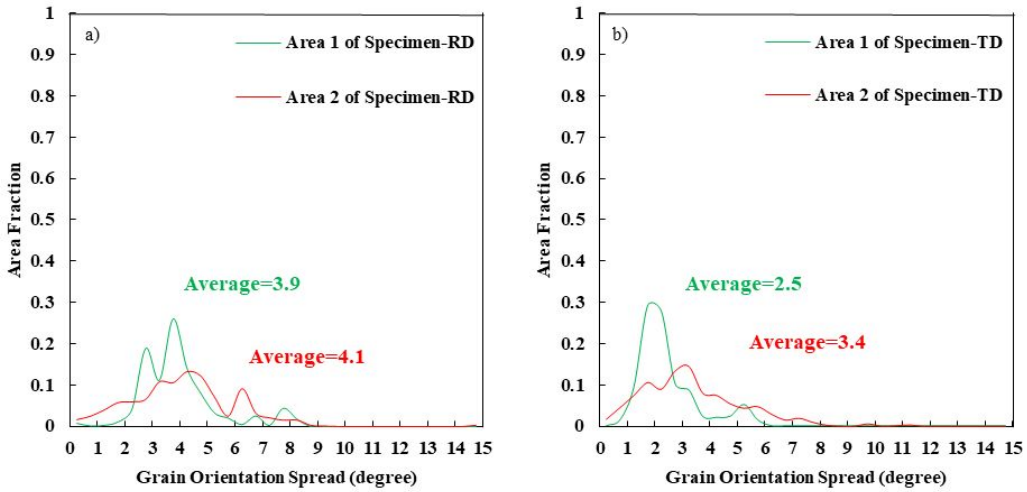

Fig. 6: Grain Orientation Spread for areas 1 and 2 of a) specimen-RD and b) specimen-TD.

In order to have a statistical analysis of texture, the texture evolution of areas 1 and 2 will be studied together from the combination of EBSD data.

3.2.1 Texture evolution of areas 1 and 2

The initial material has a typical rolled texture of BCC materials, with γ fiber as the main texture component (Fig. 7a). The γ fiber contains mainly the $\{111\}\langle 112\rangle$ and $\{111\}\langle 110\rangle$ orientations knowing that the intensity of $\{111\}\langle 110\rangle$ is lower than that of $\{111\}\langle 112\rangle$.

Compared to the initial material, the γ fibers presented in the areas 1 and 2 of both specimens become incomplete with the disappearance of the $\{111\}\langle 110\rangle$ components and the decrease of the spreading of the $\{111\}\langle 112\rangle$ orientations (Fig. 7b and c). This should be attributed to the statistical

problem without enough grains presented in the analysis areas but also to the texture evolution. In addition, some {221}⟨uvw⟩ orientations with the formation of a small part of {221} fiber are observed. In the areas 1 and 2, it exists also the {323}⟨533⟩ and {112}⟨110⟩ orientations. All these newly observed orientations correspond to a rotation around the <110> axis from {111}⟨110⟩ or {111}⟨112⟩ component of γ fiber. Indeed, it is known that the <110> axes are the normal directions of the slip planes in bcc materials. Therefore, the formation of new orientations is mainly due to the dislocation slip.

Moreover, and as already discussed above, some components of γ fiber presented in these areas of both specimens have a small orientation spread compared to the initial material. Most of the components have a spread towards the {221}⟨uvw⟩ orientations instead of a complete spread all around them. This corresponds to a deformation with few number of activated dislocation slip systems, which depends on the stress/strain state. At the same time, the average GOS of areas 1+2 is of about 4.0° and 3.0° for specimen-RD and TD, respectively. These values are still less than 5° which indicates a weak deformation associated with a few number of slip systems.

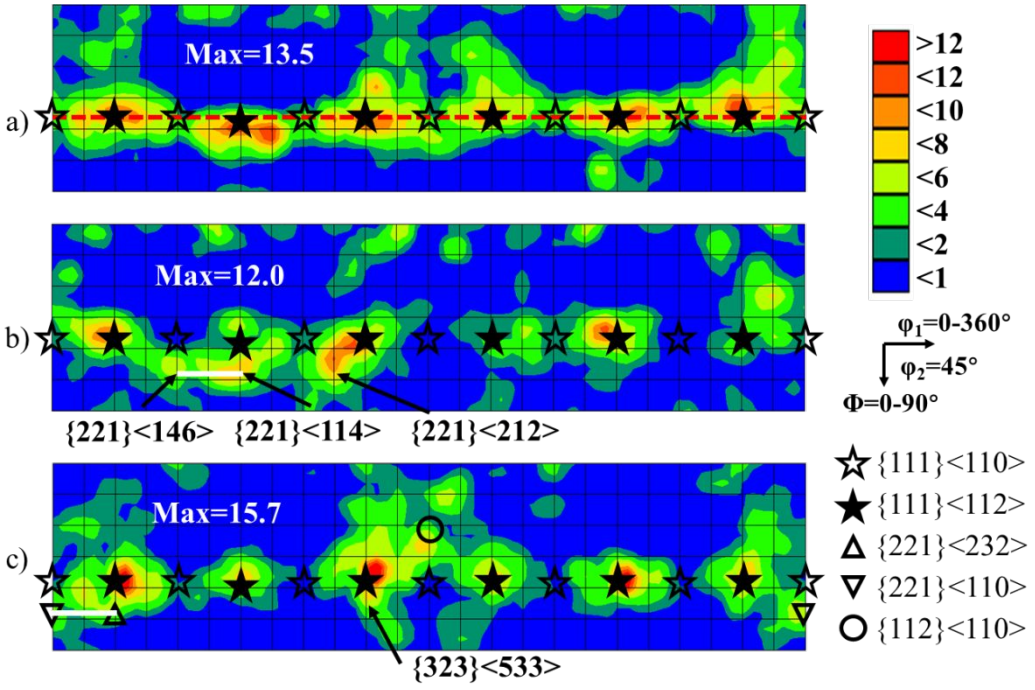

Fig. 7: ODF section plots (φ_2=45°) for a) initial material, b) areas 1+2 of specimen-RD, and c) areas

1+2 of specimen-TD; red dotted and white lines indicates the positions of γ and {221} fibers, respectively.

3.2.2 Texture evolution of area 3

For both specimens, incomplete γ fiber could be observed in area 3, and this corresponds to a statistical problem (Fig. 8a and b). In addition, the incomplete {110} fiber which is not found in initial material and in areas 1+2, is observed in the area 3 of both specimens. This {110} fiber starts from {110}⟨225⟩ to Goss {110}⟨001⟩ for specimen-RD, and from {110}⟨110⟩ to {110}⟨111⟩ for specimen-TD. For the two samples, the misorientations between the main components of the γ fiber and of the {110} fiber correspond to a rotation of 35° around ⟨110⟩ axis (Fig. 8c and d).

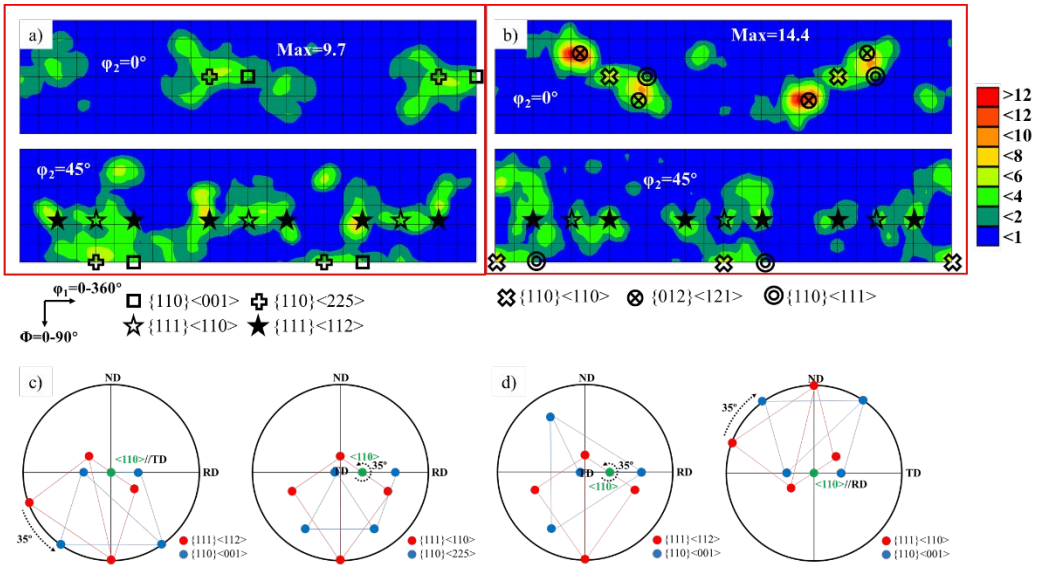

Fig. 8: ODF section plots (φ_2=0° and φ_2=45°) for area 3 of a) specimen-RD and b) specimen-TD. Illustration of rotation relationships between the main components of the γ fiber and of the {110} fiber with the {111} pole figures, for c) specimen-RD and d) specimen-TD.

For detailed study and verification, areas 3 of other specimen-RD and specimen-TD were analyzed

with high resolution (0.5 µm as the step size). At the extremity of cutting edge where shear effect from punch and die is strong, most of the ribbon grains have a $\{110\}\langle uvw\rangle$ orientation (Fig. 9a). However, it exists always some trace areas with the $\{111\}\langle uvw\rangle$ orientations around $\{110\}\langle uvw\rangle$ area. Meanwhile, the formation of some micro-shear bands in the grains were observed in area 3 of both specimens (Fig. 9b, e and f). The angles between the elongated direction of original grain and tilted direction of shear bands are about 35°.

The texture of grains including shear bands inside were also analyzed by ODF. For specimen-RD, the formation of shear bands correspond to the formation of Goss orientation from the $\{111\}\langle 112\rangle$ grains (Fig. 9b and c). The presence of shear bands with Goss orientation inside the $\{111\}\langle 112\rangle$ were also observed in the cold rolled steels as a geometric softening effect [21]. For specimen-TD, the formation of shear bands with $\{110\}\langle 110\rangle$ orientation in the $\{111\}\langle 110\rangle$ grains was also observed (Fig. 9d and e). All these shear bands lead to the formation of $\{110\}\langle uvw\rangle$ orientations from the $\{111\}\langle uvw\rangle$ ones. Meanwhile, the inverse evolution of texture from $\{110\}\langle uvw\rangle$ to $\{111\}\langle uvw\rangle$ grain could be also observed with the formation of shear bands (Fig. 9f and g). This inverse change of texture by formation of shear bands was also observed in the cold rolled silicon steel [22]. The relationship between the orientation of original grains and that of observed shear bands in this study always correspond to a rotation of 35° around the $\langle 110\rangle$ axis between them. Therefore, the formation of shear bands is one of the main deformation mechanisms presented in the area 3 with a sudden change of grain orientation. In the area 3 after punching, the relatively higher fraction of $\{110\}\langle uvw\rangle$ orientations compared to the $\{111\}\langle uvw\rangle$ orientations, should be attributed to the higher fraction of $\{111\}\langle uvw\rangle$ orientations in initial material, which leads, with a greater probability, to the formation of $\{110\}\langle uvw\rangle$ shear bands in $\{111\}\langle uvw\rangle$ grains.

Moreover, the continuum orientation spread between $\{110\}\langle uvw\rangle$ and $\{111\}\langle uvw\rangle$ as shown in the ODF sections (Fig. 9c, d and g) should correspond to the texture evolution, by dislocation slip, within grains and shear bands. This is in agreement with the existence of color gradient in both original grains and their shear bands. In addition, the existence of dislocation slip in the shear bands has been also observed in the cold rolled silicon steel [22].

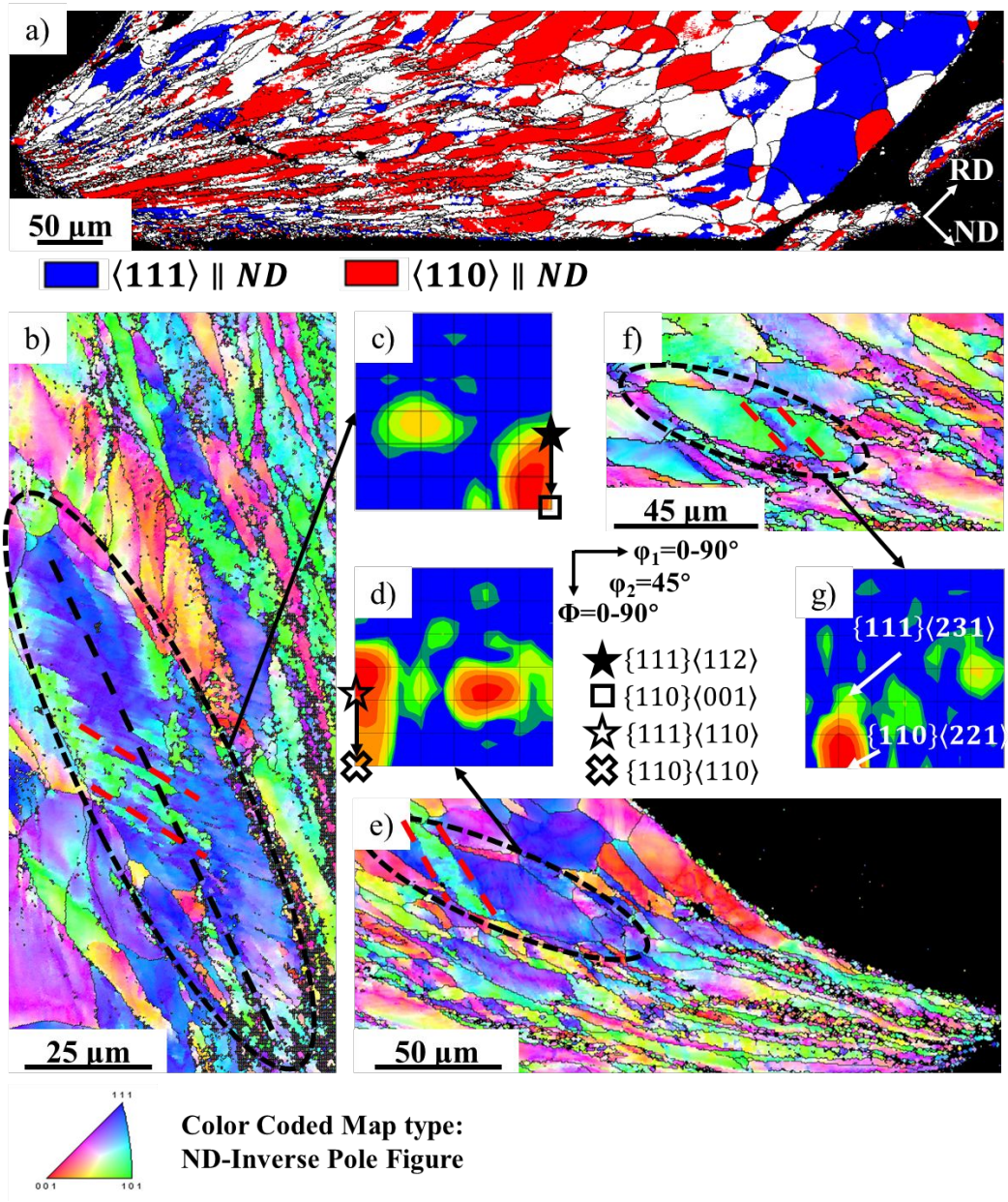

Fig. 9: a) Crystal Direction map (tolerance=15°) of area 3 cropped from another specimen-RD with a high resolution (step size: 0.5 µm); b) IPF+IQ map of shear band area in the specimen-RD with a high

resolution (step size: 0.2 μm); c) ODF section plots (φ_2=45°) for the black dotted zone in b); d) ODF section plots (φ_2=45°) for the black dotted zone in e); e) IPF+IQ map of area 3 in another specimen-TD with a high resolution (step size: 0.5 μm); f) IPF+IQ map of shear band area in the specimen-TD with a high resolution (step size: 0.5 μm); g) ODF section plots (φ_2=45°) for the black dotted zone in f); RD and ND in a) represent the sample directions after punching; black dotted line in b) shows the elongated direction of the deformed grain; red dotted lines show the locations and inclined directions of shear bands.

4. Conclusion

With a worn punch tool, the cutting edges of samples are strongly bent, and could be divided into three areas.

The bent effect is negligible in the area 1. The bent angle of area 2 varies continuously, and the EBSD data were corrected with PRM. The whole areas 3 of specimens-RD and TD are bent with a cumulative angle (45°), and the EBSD data were corrected with a direct rotation of the sample system.

Then, the deformation mechanisms and the texture evolution at the edges of the punched silicon steel were studied. The observations could be summarized as follow:

In area 1 and 2 of specimens-RD,-TD, the grains with the $\{111\}\langle uvw\rangle$ orientation rotate towards the $\{211\}\langle uvw\rangle$ orientations by dislocation slip.

Areas 3 of the two specimens contain a large number of ribbon grains at the extremity of the cutting edge. Most of ribbon grains have a $\{110\}\langle uvw\rangle$ or a $\{111\}\langle uvw\rangle$ orientation. These grains with different fiber-orientations appear alternately and cross with each other. Moreover, the main deformation mechanisms in these areas are dislocation slip and formation of shear bands. The formation of shear

bands leads to a change of texture between the $\{111\}\langle uvw\rangle$ and the $\{110\}\langle uvw\rangle$ orientations, and the dislocation slip leads to the orientation spread around these two main orientations. All these observations illustrate that the formation of shear band is the main deformation mechanism and that results in the formation of the $\{110\}$ fiber from the γ fiber.

Acknowledgments: This work was supported by the National Natural Science Foundation of China (Grant No. 51801141) and the Fundamental Research Funds for the Central Universities (WUT: 2019IVB015). The authors would also acknowledge the support from 111 Project (B17034) and Innovative Research Team Development Program of Ministry of Education of China (IRT_17R83).

References

[1] K. Honda, On magnetization of single crystals of iron, *Sci. Rep. Tohoku Imp. Univ.*, 15(1926).

[2] H. Liu, Z. Liu, C. Li, G. Cao and G. Wang, Solidification structure and crystallographic texture of strip casting 3 wt.% Si non-oriented silicon steel, *Mater. Charact.*, 62(2011), No.5.

[3] Y. Xu, Y. Zhang, Y. Wang, C. Li, G. Cao, Z. Liu and G. Wang, Evolution of cube texture in strip-cast non-oriented silicon steels, *Scripta Mater.*, 87(2014).

[4] M. Mehdi, Y. He, E. J. Hilinski and A. Edrisy, Effect of skin pass rolling reduction rate on the texture evolution of a non-oriented electrical steel after inclined cold rolling, *J. Magn. Magn. Mater.*, 429(2017).

[5] M. Sanjari, Y. He, E. J. Hilinski, S. Yue and L. A. Kestens, Texture evolution during skew cold rolling and annealing of a non-oriented electrical steel containing 0.9 wt% silicon, *J. Mater. Sci.*, 52(2017), No.6.

[6] M. Mehdi, Y. He, E. J. Hilinski, L. A. Kestens and A. Edrisy, The evolution of cube ({001}<

100>) texture in non-oriented electrical steel, *Acta Mater.*, 185(2020).

[7] H. Jiao, Y. Xu, H. Xu, Y. Zhang, W. Xiong, R. Misra, G. Cao, J. Li and J. Jiang, Influence of hot deformation on texture and magnetic properties of strip cast non-oriented electrical steel, *J. Magn. Magn. Mater.*, 462(2018).

[8] H.-Z. Li, H.-T. Liu, Z.-Y. Liu, H.-H. Lu, H.-Y. Song and G.-D. Wang, Characterization of microstructure, texture and magnetic properties in twin-roll casting high silicon non-oriented electrical steel, *Mater. Charact.*, 88(2014).

[9] H.-T. Liu, Z.-Y. Liu, Y. Sun, Y.-Q. Qiu, C.-G. Li, G.-M. Cao, B.-D. Hong, S.-H. Kim and G.-D. Wang, Formation of {001}< 510> recrystallization texture and magnetic property in strip casting non-oriented electrical steel, *Mater. Lett.*, 81(2012).

[10] Y. Sha, C. Sun, F. Zhang, D. Patel, X. Chen, S. Kalidindi and L. Zuo, Strong cube recrystallization texture in silicon steel by twin-roll casting process, *Acta Mater.*, 76(2014).

[11] N. Zhang, P. Yang and W.-M. Mao, Through process texture evolution of new thin-gauge non-oriented electrical steels with high permeability, *J. Magn. Magn. Mater.*, 397(2016).

[12] G. Sahoo, C. Singh, M. Deepa, S. Dhua and A. Saxena, Recrystallization behaviour and texture of non-oriented electrical steels, *Mater. Sci. Eng., A*, 734(2018).

[13] F. Ossart, E. Hug, O. Hubert, C. Buvat and R. Billardon, Effect of punching on electrical steels: experimental and numerical magneto-mechanical analyses, [in] *Proceedings of the 2000 IEEE International Magnetics Conference (INTERMAG)*, 2000, 556-556.

[14] H. Weiss, N. Leuning, S. Steentjes, K. Hameyer, T. Andorfer, S. Jenner and W. Volk, Influence of shear cutting parameters on the electromagnetic properties of non-oriented electrical steel sheets, *J. Magn. Magn. Mater.*, 421(2017).

[15] A. Saleem, D. Goldbaum, N. Brodusch, R. Gauvin and R. R. Chromik, Microstructure and mechanical property connections for a punched non-oriented electrical steel lamination, *Mater. Sci. Eng., A*, 725(2018).

[16] T. B. Penelle, Determination of the total texture, *Metall. Mater. Trans. A*(1993).

[17] D. Field, L. Bradford, M. Nowell and T. Lillo, The role of annealing twins during recrystallization of Cu, *Acta Mater.*, 55(2007), No.12.

[18] J. Mackenzie, Second paper on statistics associated with the random disorientation of cubes, *Biometrika*, 45(1958), No.1-2.

[19] J. Mason and C. Schuh, The generalized Mackenzie distribution: Disorientation angle distributions for arbitrary textures, *Acta Mater.*, 57(2009), No.14.

[20] X. Jin, B.-q. Fu, C.-l. Zhang and W. Liu, Evolution of the texture and mechanical properties of 2060 alloy during bending, *Int. J. Miner. Metall. Mater.*, 22(2015), No.9.

[21] T. Nguyen-Minh, J. Sidor, R. Petrov and L. Kestens, Shear banding and its contribution to texture evolution in rotated Goss orientations of BCC structured materials, [in] *Proceedings of the IOP Conference Series: Materials Science and Engineering*, 2015, 012023.

[22] D. Dorner and S. Zaefferer, Microstructure and texture of shear bands in cold rolled silicon steel single crystals of Goss orientation, [in] *Proceedings of the Solid State Phenomena*, 2005, 239-244.